Droplet features extraction with a dynamic active contour for MIG/MAG welding modelling.

Jean-Pierre Planckaert, El-Hadi Djermoune, David Brie, Francis Briand, Frédéric Richard

DROPLET FEATURES EXTRACTION WITH A DYNAMIC ACTIVE CONTOUR FOR MIG/MAG WELDING MODELLING

J.-P. Planckaert*, E.H. Djermoune*, D. Brie*, F. Briand†, F.-P. Richard†

* *CRAN – CNRS UMR 7039, Université Henri Poincaré, Nancy 1, BP 239, 54506 Vandœuvre-les-Nancy Cedex, France*
jean-pierre.planckaert@cran.uhp-nancy.fr, el-hadi.djermoune@cran.uhp-nancy.fr, david.brie@cran.uhp-nancy.fr
† *CTAS/AIR LIQUIDE, 13 rue d'Epluches, BP 70024 Saint Ouen l'Aumône, 95315 Cergy-Pontoise Cedex, France*
francis.briand@airliquide.com, frederic-p.richard@airliquide.com

Keywords: MIG/MAG welding, modelling, active contour, *greedy* algorithm.

Abstract

In this paper, we present a discrete contour model used to follow the dynamical behaviour of a molten metal drop in short arc welding. Good results are achieved on experimental movies as drop edges are well detected. This approach enables the estimation of the relevant variables in the establishment of a model of MIG/MAG welding in short arc mode.

1 Introduction

The Metal Inert Gas/Metal Active Gas (MIG/MAG) welding is an arc welding process in which additional metal is brought by a roll of wire line and is molten by Joule effect and an electric arc [1]. In the short arc mode, the weld is made by successive drops. An inert gas, generally argon based gas (MIG welding), or active gas, generally CO_2 based gas (MAG welding) is used as plasma for electric arc outbreak and as protective atmosphere for metal at high temperature, avoiding contamination of the metal by oxygen and nitrogen. The welding generator supplies the electric energy required for melting and for arc outbreak and sustainment between wire and workpieces to weld. It works according to two distinct control modes:

- the arc mode in which the voltage delivered by the generator is regulated to reach a set point decided by the welder;
- the short circuit mode in which the current follows a pre-defined law.

The general framework of this study concerns the modeling of the MIG/MAG welding process for a metal transfer in short arc mode. It aims at providing a model of the whole system including wire, gas, arc, sheet metal and control. Such a model is expected to give some insights into the understanding of the welding process and, consequently, to lead to improved control strategy.

The molten metal drop detachment from an electrode in gas metal arc welding involves complex interactions between different physical phenomena [2, 3, 4, 5, 6] which have been used to propose an hybrid model accounting for the switching from the arc mode to the short-circuit mode [7]. The next aspect of the study is the development of a model identification method. This includes an experimental aspect consisting in building a database from which model identification will be achieved.

All the recordings are realised on a test bed equipped with an acquisition system for measuring voltage, current, wirefeed velocity. All these measurements are sampled synchronously with a high speed video system operating at 12500 frames/s. The video system is used to measure quantities such as drop position, volume or liquid-solid border relevant for the model identification. In that respect it is necessary to perform a segmentation of the images. However our images are too complex to expect local, low level operations to generate perfect primitives. Higher level features have to be used to get a better delineation of objects. We chose to use deformable models which adapt to the data.

The paper is organised as follows. In section 2, a brief description of the physical aspect of Gas Metal Arc Welding (GMAW) in the short arc mode is given. After having introduced the main forces acting in the process, we chose the variables of interest in order to implement a model of the system. Next, in section 3, we introduce the active contour methodology allowing us to observe these variables. Experimental results are given in section 4. They show the effectiveness of the approach to give access to the dynamic of the chosen variables. Finally, the conclusion raises some issues to be developed in future work.

2 GMAW system in short arc mode

2.1 General description

Short-circuiting metal transfer, is a metal transfer whereby a continuously fed wire electrode is deposited during electrical short-circuits. The transfer of a single molten droplet of electrode occurs during the shorting phase of the transfer cycle when physical contact with the molten weld pool occurs.

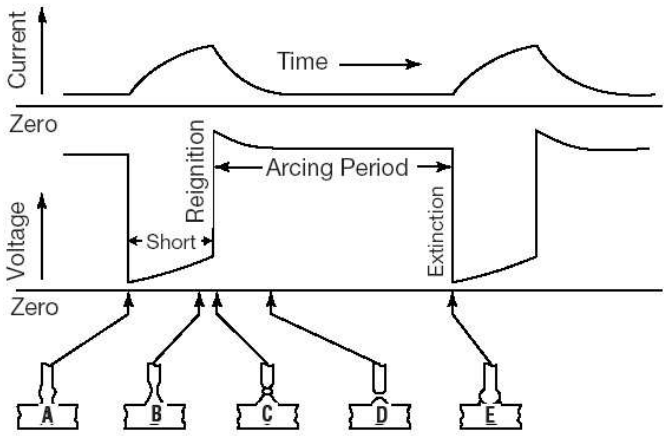

Figure 1: Oscillograms and sketches of short circuiting transfer.

Figure 1 illustrates the time evolution of a droplet together with the corresponding arc voltage and welding current. Metal transfer goes through five steps:

- A: The electrode makes physical contact with the molten pool. The arc voltage approaches zero and the current level increases. The rate of rise to the peak current is affected by the amount of applied inductance.
- B: This point demonstrates the effect of electromagnetic forces that are applied around the electrode. This force pinches the electrode.
- C:This is the point where the bridge of molten metal explodes. The droplet is forced from the tip of the electrode to the welding pool.
- D: The molten droplet reforms while current is at its background level.
- E: The electrode is once again making contact with the pool, preparing for the transfer of another droplet.

The area of the welding arc, sketched on figure 2, is a region of high complexity that is comprised of physical forces and chemical reactions. The interaction of the components of the arc affects metal transfer and the quality of the finished weld. The behavior of the arc is influenced by: the type and the diameter of the filler metal, the base metal conditions, the shielding gas,the welding parameters (voltage and current), the interaction of physical forces.

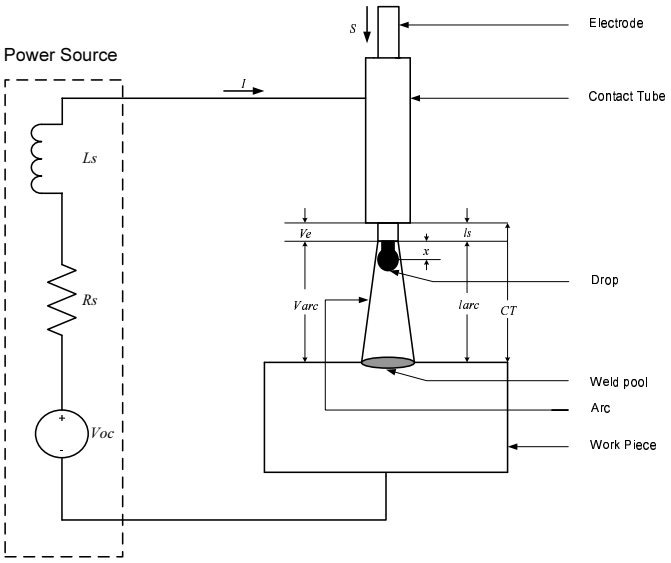

Figure 2: Welding system sketch.

The phenomenon of metal transfer in short arc welding can be seen as an hybrid system as figured on figure 3. Indeed it presents two continuous states: a first one during which the droplet grows and a second one during which the electrode is in physical contact with the workpiece. The jump between the two states is linked to the accomplishment of a guard condition:

- *cond 1*: The contact-tube to workpiece distance is inferior to the electrode extension plus droplet length,
- *cond 2*: the molten metal bridge diameter is inferior to a threshold fixed by electrical and material laws.

In each state, a set of differential equations drives the process behaviour. These equations stem from power source characteristics and the set of forces acting on a droplet. Two categories of forces can arise in our process: detach-

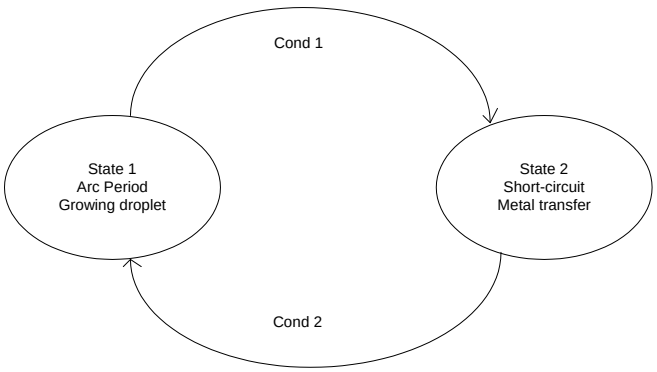

Figure 3: Short-circuiting GMAW working sketch.

ing ones and retaining ones. Three forces have been identified as relevant:

1. The gravitational force.
2. The electromagnetic force which results from diverging or converging current flow within the electrode. When the current path diverges in the drop, the Lorentz force presents an axial component acting, normal to the current path and creating a detaching force, and an orthoradial component which squeezes the molten droplet at the end of the electrode.
3. The surface tension which is normal to the surface of a molten droplet. It serves to support the form of a molten droplet. There is always an inward pull acting to retain the droplet on the electrode.

The expression of these forces is given in the next paragraph. More generally, the reader is reported to references [2, 3, 4, 5, 6] for a complete description of the welding physics.

2.2 Model of droplet growth

We present here a simple model of droplet growth during arcing period. Through this work we aim at checking some ideas often encountered when dealing with welding. The forces acting on the drop are:

- gravitational force

$$F_g = \frac{4}{3}\pi r_d^3 \rho_w g \tag{2.1}$$

  where r_d is the droplet radius, ρ_w the electrode density and g is the gravity acceleration.

- axial electromagnetic force

$$F_{em} = \frac{\mu_0 I^2}{4\pi}\left[\ln\frac{r_d \sin\theta}{r_w} - \frac{1}{4} - \frac{1}{1-\cos\theta} + \frac{2}{(1-\cos\theta)^2}\ln\frac{2}{1+\cos\theta}\right] \tag{2.2}$$

  where μ_0 is the permeability of free space, I the current and r_w the electrode radius.

- surface tension force

$$F_S = 2\pi r_w \gamma \tag{2.3}$$

  where γ is the surface tension of liquid steel.

We have used these expressions of forces to write a state-space representation of the governing differential equations of droplet growth. State variables are:

- $x_1 = x$: droplet displacement,
- $x_2 = \dot{x}$: droplet velocity,
- $x_3 = I$: current,
- $x_4 = l_s$: stickout,
- $x_5 = m_d$: droplet mass.

State equations are:

$$\dot{x}_1 = x_2 \tag{2.4}$$

$$\dot{x}_2 = \frac{F_g + F_{em} + F_S}{x_5} \tag{2.5}$$

$$\dot{x}_3 = \left[V_{oc} - (R_a + R_S)x_3 - V_0 - E_a(CT - x_4) - \left[x_4 + x_1 + \left(\frac{3x_5}{4\pi.\rho_w}\right)^{\frac{1}{3}}\right]\rho.x_3\right]\frac{1}{L_S} \tag{2.6}$$

$$\dot{x}_4 = S - \frac{C_2.\rho.x_3^2.x_4 + C_1.x_3}{\pi.r_{w^2}} \tag{2.7}$$

$$\dot{x}_5 = (C_2.\rho.x_3^2.x_4 + C_1.x_3)\rho_w \tag{2.8}$$

Where V_0 is the arc voltage constant,V_{oc} the open circuit voltage, E_a the arc length factor, CT the contact tube to workpiece distance, R_a the arc resistance, R_S the source resistance and ρ the electrode resistivity. C_1 and C_2 will be presented in the sequel.

In order to implement the model of the system shown on figure 3, offering a good agreement with the practical work of the process, it is necessary to supervise some variables of interest during a normal operation of the testing bed. Indeed, we need the dynamic behaviour of the volume of the drop, the center of gravity and the liquid-solid border synchronously with arc voltage and welding current. So an experimental database has been built with electrical measurements and high speed videos. The work presented here aims at extracting information concerning the droplet from videos. In this purpose we decided to use active contours.

3 Active contour segmentation

Active contour models introduced by Kass and Witkins [8] have rapidly seduced the scientific community by their ability to efficiently combine both the available *a priori* knowledge about the structure of interest and local correspondance with the image features [9, 10, 11]. Their principle is to evolve from an initial contour to equilibrium which corresponds to the edges of the object to detect.

Active contour models are also known as *snakes* or *minimizing curves*. This is a semi-interactive method in which the user puts an initial contour in the image (near the shape to find) and this one will be deformed by the action of several energies. The contour will evolve searching the position of lowest local energy.

In its continuous form, the snake is described by a parametric curve $v(s) = [x(s), y(s)]^t$ with $s \in [0,1]$ and $v(0) = v(1)$ for a closed contour. Its total energy can be written as:

$$E_{snake} = \int_0^1 \Big[E_{int}(v(s)) + E_{im}(v(s)) + E_{ext}(v(s))\Big] ds \quad (3.1)$$

where E_{int}, E_{im} and E_{ext} denote internal, image and external energies, respectively. The internal energy depends only on the contour shape. It is given by:

$$E_{int}(v(s)) = \alpha E_{cont}(v(s)) + \beta E_{curv}(v(s)) = \alpha \left(\frac{dv}{ds}\right)^2 + \beta \left(\frac{d^2v}{d^2s}\right)^2 \quad (3.2)$$

The first order term drives continuity while the second order term controls curvature.

The potential energy related to the image can be written as:

$$E_{im}(v(s)) = -\lambda(s)|\nabla I(v(s))|^2 \quad (3.3)$$

This energy qualifies the elements towards which we want to attract the contour on the image. In the segmentation framework it corresponds to the lines of high gradient.

The external energy is user defined in accordance with the problem specificities. For instance we can impose a minimal distance between two consecutive points of the snake.

Without an external energy and when high gradient lines are sought we can write:

$$E_{snake}(v(s)) = \alpha E_{cont}(v(s)) + \beta E_{curv}(v(s)) + \gamma E_{im}(v(s)) \quad (3.4)$$

The triplet (α, β, γ) enables to strike a balance between different energies. In the continuous domain, the energy equation of a contour C can be expressed by:

$$E_{snake} = \int_C \left[-\gamma(s)|\nabla I(v(s))|^2 + \alpha \left(\frac{dv}{ds}\right)^2 + \beta \left(\frac{d^2v}{d^2s}\right)^2\right] ds \quad (3.5)$$

In a discrete approach, the contour is a list of points M_i, $i \in [1, n]$. The energy of the snake is assimilated to the sum of the energies associated with the n points defining it:

$$E_{snake} = \sum_{i=1}^{n} \Big[\alpha E_{cont}(M_i) + \beta E_{curv}(M_i) + \gamma E_{im}(M_i)\Big] \quad (3.6)$$

In order to minimize E_{snake}, we determine the list of n points constituting C. To achieve this goal we have chosen to implement the *greedy* algorithm [12, 13, 14].

In this approach the derivatives in equation 3.5 have to be approximated by finite differences. If $v_i = [x_i, y_i]^t$ is a point of the contour, we write:

$$\left|\frac{dv_i}{ds}\right|^2 \approx |v_i - v_{i-1}|^2 = (x_i - x_{i-1})^2 + (y_i - y_{i-1})^2 \quad (3.7)$$

and

$$\left|\frac{d^2v_i}{ds^2}\right|^2 \approx |v_{i-1} - 2v_i + v_{i+1}|^2 = (x_{i-1} - 2x_i + x_{i+1})^2 + (y_{i-1} - 2y_i + y_{i+1})^2 \quad (3.8)$$

Two assumptions have been made here:

- The points are spaced at unit intervals. If the points are evenly spaced, then equation 3.7 should be divided by d^2, where d is the distance between points and equation 3.8 by d^4.
- If the points are not evenly spaced, the first derivative term will be divided by d_i^2 where d_i is the distance between points i and $i-1$.

The third term in equation 3.4 (E_{im}) is the image force, which is the gradient magnitude at each point in the image, intensity being coded as an eight bit integer.

The *greedy* algorithm is iterative. During each iteration, a neighborhood of each point is examined and the point in the neighborhood giving the smallest value for the energy term is chosen as the new location of the point as represented on figure 4.

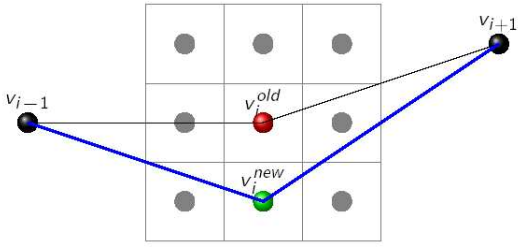

Figure 4: *Greedy* algorithm behaviour.

Our final aim is to get information on the drop evolution. To achieve it, we have acquired a set of movies which are lists of images. Consequently, the idea is to use the detected contour at image $(k-1)$ to initialize the one at image k.

4 Experimental results

4.1 Snake following droplet growth

The example shown here corresponds to a movie acquired at 12500 frames per second using a resolution of 512×256.

On figure 5 we can see the user-defined initial contour. The greedy algorithm is applied on the first image until convergence. Then, as mentioned before, the contour obtained serves as an initialization for frame 2, and so on. For instance, the results obtained for frames 15, 30, 45, 60, 75, 90 and 105 are shown on figures 5. As we can see, the algorithm leads to a good detection of the drop edge. Even when the droplet is in contact with the welding pool, the active contour is still efficient and leads to a good segmentation.

From these results, it is now possible to determine the dynamical behaviour of some variables as, for instance, the surface and the gravity center displacement of the droplet as shown on figure 6. The phase between image 1 and image 60 corresponds to the droplet growth since the surface increases. This phase is followed by the physical contact between the droplet and the weld pool which allows the metal transfer and the decrease in the surface. The same observations can be made concerning the displacement.

The next paragraph presents a comparison between the physical and the experimental dynamics of the process, the later being obtained from the active contour. This comparison is made only in the droplet growth period because we still have problems to reinitialise the contour after contact break between the end of the electrode and the pool.

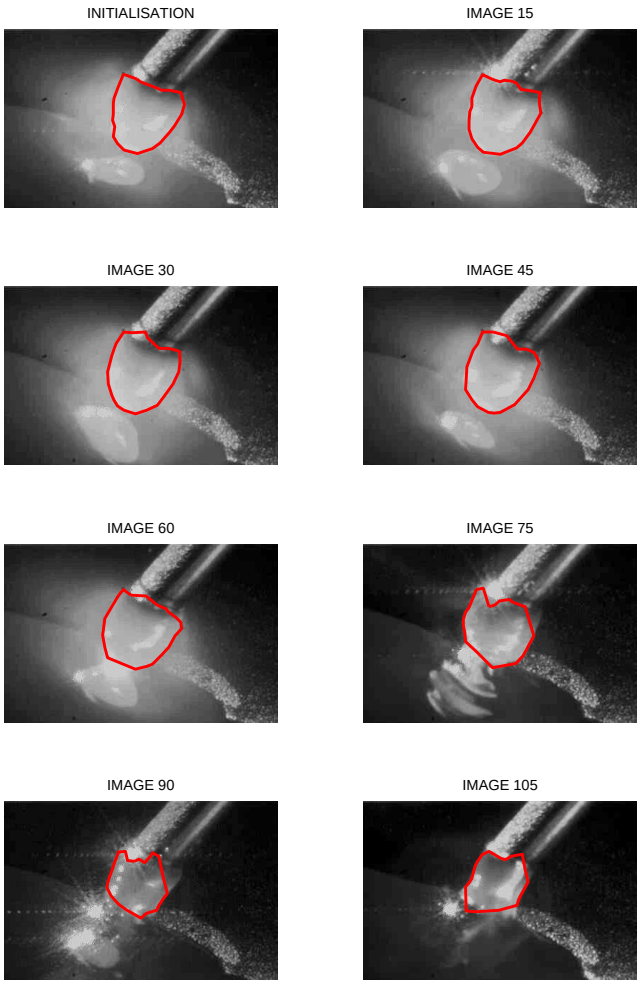

Figure 5: Evolution of the active contour over the set of images.

4.2 Comparison between model and experimental data

The state space representation introduced in section 2 is used in a simulator and, thanks to the Matlab differential-algebraic equations solver, we have obtained dynamics of the state variables shown on figure 7. The curves correspond to an arcing period while the droplet is growing at the end of the electrode. As we can see, the droplet displacement (more precisely its center of gravity displacement) increases simultaneously with its mass insofar as molten metal is added to the drop at each time step because of the physical law driving the melting rate M_R:

$$M_R = C_2 I^2 l_s \rho + C_1 I \tag{4.1}$$

where C_1 and C_2 are constants fixed to strike a balance between Joule effect and arc heat fusions.

The current presents an exponential decrease as presented in figure 1. The decrease rate is controlled by the generator inductance L_S shown in figure 2.

The video on which we have applied our algorithm takes place during the droplet growth too. As expected on figure 8, we can observe an increase of the droplet surface as well as a displacement of the center of gravity downward.

We have used the first values of droplet surface and displacement obtained with the estimated contour on image 1 to initialize the simulator. We notice that the observed variables present an order of magnitude close to experimental ones. Consequently we can assume that the main influences represented by the three forces acting on the drop are sufficient for modelling this period. Nevertheless, the dynamic is not the same which indicates that some other parameters of the physical model have to be tuned more precisely in order to fit to experimental results. For instance C_1 and C_2 have to be determined experimentally as they control the amount of metal to be molten through the expression of the melting rate.

5 Conclusion

A discrete contour model has been developed to follow the dynamical behaviour of a molten metal drop in short

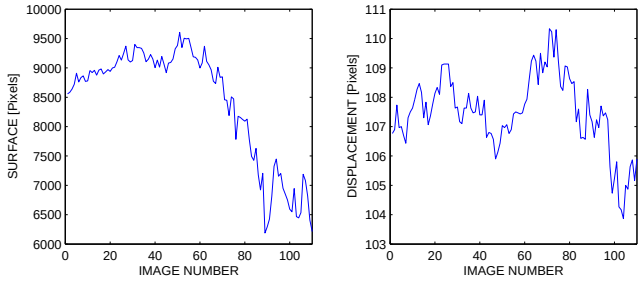

Figure 6: Evolution of the droplet surface and its y-axis displacement.

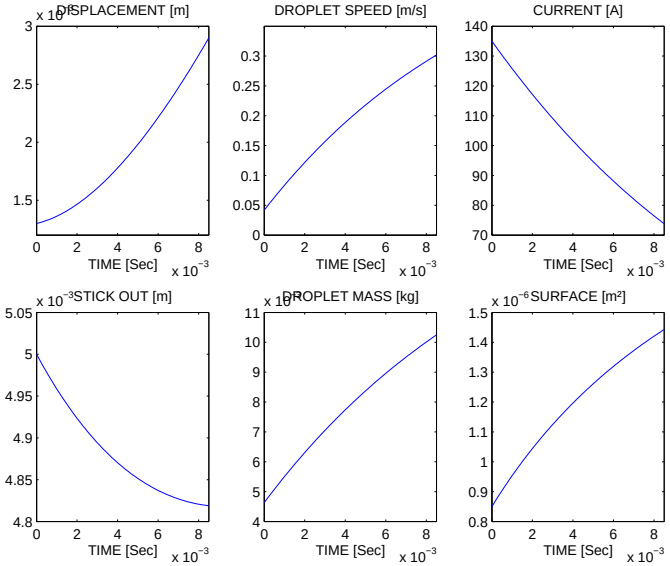

Figure 7: Simulator results.

arc welding. Good results are achieved on experimental movies as the drop edges are well detected. This approach enables one to estimate the relevant variables in the establishment of a model of MIG/MAG welding in short arc mode.

A simplified droplet growth dynamic model has also been presented. Model predictions are consistent with experimental data even if the tuning of some parameters have to be improved.

The discrete contour algorithm will help getting further insight in gas metal arc welding:

- information on droplets surface and displacement will be compared to those given by simulators so as to improve the agreement between theory and experience, during a complete period including arc time and short-circuit time.
- empirical tendency of some variables of interest will be studied in the establishment of some basic statistical laws such as weld quality, drop size, spatters, etc.

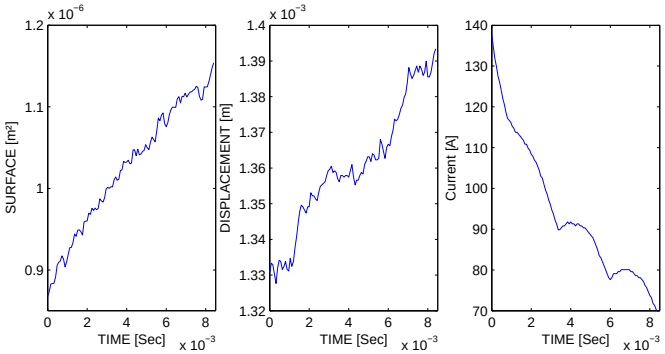

Figure 8: Experimental measurements.

References

[1] S. Adolfsson, A. Bahrami, G. Bolmsjö, and I. Claesson, "On-line quality monitoring in short-circuit gas metal arc welding," *Welding Research Supplement*, vol. 78, no. 2, pp. 59–73, february 1999.

[2] L. Jones, T. Eagar, and J. Lang, "A dynamic model of drops detaching from a gas metal arc welding electrode," *Applied Physics*, vol. 31, pp. 107–123, 1998.

[3] ——, "Magnetic forces acting on molten drops in gas metal arc welding," *Applied Physics*, vol. 31, pp. 93–106, 1998.

[4] K. Moore, D. Naidu, R. Yender, and J. Tyler, "Gas metal arc welding control: part i -modeling and analysis-," in *Proc. 2nd World Congress of Nonlinear Analysis*, ser. Nonlinear Analysis, Theory, Methods & Applications, vol. 30, 1997, pp. 3101–3111.

[5] A. Watkins, H. Smartt, and J. Johnson, "A dynamic model of droplet growth and detachment in GMAW," in *Third International Conference On Trends In Welding Research*, 1992, pp. 993–997.

[6] J. C. Amson, "Lorentz force in the molten tip of an arc electrode," *British Journal of Applied Physics*, vol. 16, pp. 1169–1179, 1965.

[7] J.-P. Planckaert, E.-H. Djermoune, D. Brie, F. Briand, and F.-P. Richard, "Modélisation du soudage MIG/MAG en mode short-arc," Centre de Recherche en Automatique (CRAN) / Centre Technique des Applications du Soudage (CTAS), Tech. Rep., June 2005, 35 pages.

[8] M. Kass, A. Witkin, and D. Terzopoulos, "Snakes : Active contour models," *International Journal of Computer Vision*, vol. 55, pp. 321–331, 1988.

[9] H. Delingette and J. Montagnat, "Topology and shape constraints on parametric active contours," INRIA, Sophia Antipolis, Report 3880, january 2000.

[10] L. D. Cohen, "On active contour models and ballons," *Computer Vision, Graphics, and Image Processing: Image Understanding*, vol. 53, no. 2, pp. 211–218, 1991.

[11] H. T. Nguyen, R. v. d. B. M. Worring, and A. W. M. Smeulders, "Tracking nonparameterized object contours in video," *IEEE Transactions on Image Processing*, vol. 11, no. 9, pp. 1–11, september 2002.

[12] D. J. Williams and M. Shah, "A fast algorithm for active contours and curvature estimation," *Computer Vision, Graphics, and Image Processing: Image Understanding*, vol. 55, no. 1, pp. 14–26, 1992.

[13] P. Ladret, B. Latombe, and F. Granada, "Active contour algorithm: An attractive tool for snow avalanche analysis," *Signal Processing*, vol. 79, pp. 197–204, 1999.

[14] S. Lobregt and M. Viergever, "A discrete dynamic contour model," *IEEE Transactions on Medical Imaging*, vol. 14, no. 1, pp. 12–24, march 1995.